Microporous Materials Constructed from the Interpenetrated Coordination Networks. Structures and Methane Adsorption Properties

Mitsuru Kondo,† Mariko Shimamura,‡ Shin-ichiro Noro,‡ Seika Minakoshi,‡ Akiko Asami,‡ Kenji Seki,§ and Susumu Kitagawa*,†

Department of Synthetic Chemistry and Biological Chemistry, Graduate School of Engineering, Kyoto University, Yoshida, Sakyo-ku, Kyoto 606-8501, Japan; Department of Chemistry, Graduate School of Science, Tokyo Metropolitan University, 1-1 Minamiohsawa, Hachioji-shi, Tokyo 192-0397, Japan; and Energy Conversion and Storage Technology, Applied Research Center, Research and Development Department, Osaka Gas Co., Ltd. 6-19-9, Torishima, Konohana-ku, Osaka 554-0051, Japan

Received September 29, 1999. Revised Manuscript Received February 23, 2000

Five new coordination compounds with 4,4′-azopyridine (azpy), $[Mn(azpy)(NO_3)_2(H_2O)_2]\cdot 2EtOH$ (**1**·2EtOH), $[Co_2(azpy)_3(NO_3)_4]\cdot Me_2CO\cdot 3H_2O$ (**2**·Me_2CO·$3H_2O$), $[Co(azpy)_2(NCS)_2]\cdot 0.5EtOH$ (**3**·0.5EtOH), $[Cd(azpy)_2(NO_3)_2]\cdot(azpy)$ (**4**·azpy), and $[Cd_2(azpy)_3(NO_3)_4]\cdot 2Me_2CO$ (**5**·$2Me_2CO$), have been synthesized and structurally characterized. The reaction of $Mn(NO_3)_2\cdot 6H_2O$ with azpy in ethanol/acetone affords **1**·2EtOH, whose network consists of one-dimensional chains of $[Mn(azpy)(H_2O)_2]_n$. The chains are associated by hydrogen bonding to provide a *logcabin*-type three-dimensional structure, which creates about 8 × 8 Å of channels, filled with ethanol molecules. The treatment of $Co(NO_3)_2\cdot 6H_2O$ and $Co(NCS)_2\cdot 4H_2O$ with azpy produces **2**·Me_2CO·$3H_2O$ and **3**·0.5EtOH, respectively, which have a *brick-wall* and a *rhombus*-type two-dimensional networks. The reaction of $Cd(NO_3)_2\cdot 4H_2O$ with azpy affords **4**·azpy from the ethanol/H_2O media, while the reaction in the ethanol/acetone media provides **5**·$2Me_2CO$. **4**·azpy and **5**·$2Me_2CO$ form a *square-grid*- and a *herringbone*-type two-dimensional networks, respectively. The two-dimensional sheets of **4**·azpy stack without interpenetration, leading to large size of channels, which are filled with free azpy molecules. The two-dimensional networks of **2**·Me_2CO·$3H_2O$, **3**·0.5EtOH, and **5**·$2Me_2CO$ are quadruply, doubly, and triply interpenetrated, respectively. Despite the interpenetration, their networks create the microporous channels filled with guest solvent molecules. The dried compounds **2**, **3**, and **5** adsorb methane between 1 and 36 atm at 25 °C, in which **3** and **5** exhibit Langmuir-type isotherms. The inherent micropore volumes for **3** and **5** are 0.685 and 3.30 mmol/g, respectively. XRPD measurements under reduced pressure at 100 °C reveal that the channel structure of **3** is the most stable in these compounds; the observed XRPD pattern is in good agreement with that of the simulated pattern of the single-crystal model. Compounds **2** and **5** also retain the porous structures, however, their pore structures are distorted upon loss of guest included molecules.

Introduction

Design and preparation of coordination polymers with new porous frameworks are of great current interest due to their potential functionalities such as size-selective molecular adsorption,[1−13] shape-selective catalysis,[1,14,15] and ion-exchange.[16−18] There have been a wide variety of coordination polymers with microcavities, which usually accommodate guest molecules such as solvent molecules and/or counterions.[1,5,19−22,31−33] The channel structures are usually retained as far as they hold guest

* To whom correspondence should be addressed.
† Kyoto University.
‡ Tokyo Metropolitan University.
§ Osaka Gas Co., Ltd.

(1) Fujita, M.; Kwon, Y. J.; Washizu, S.; Ogura, K. *J. Am. Chem. Soc.* **1994**, *116*, 1151−1152.
(2) Yaghi, O. M.; Li, G.; Li, H. *Nature* **1995**, *378*, 703−706.
(3) Venkataraman, D.; Gardner, G. B.; Lee, S.; Moore, J. S. *J. Am. Chem. Soc.* **1995**, *117*, 11600−11601.
(4) Yaghi, O. M.; Li, H.; Groy, T. L. *J. Am. Chem. Soc.* **1996**, *118*, 9096−9101.
(5) Yaghi, O. M.; Davis, C. E.; Li, G.; Li, H. *J. Am. Chem. Soc.* **1997**, *119*, 2861−2868.
(6) Russell, V. A.; Evans, C. C.; Li, W.; Ward, M. D. *Science* **1997**, *276*, 575−579.
(7) Kondo, M.; Yoshitomi, T.; Seki, K.; Matsuzaka, H.; Kitagawa, S. *Angew. Chem., Int. Ed. Engl.* **1997**, *36*, 1725−1727.
(8) Mori, W.; Inoue, F.; Yoshida, K.; Nakayama, H.; Takamizawa, S. *Chem. Lett.* **1997**, 1219−1220.
(9) Li, H.; Eddaoudi, M.; Groy, T. L.; Yaghi, O. M. *J. Am. Chem. Soc.* **1998**, *120*, 8571−8572.
(10) Choi, H. J.; Suh, M. P. *J. Am. Chem. Soc.* **1998**, *120*, 10622−10628.
(11) Biradha, K.; Dennis, D.; MacKinnon, V. A.; Sharma, C. V. K.; Zaworotko, M. J. *J. Am. Chem. Soc.* **1998**, *120*, 11894−11903.
(12) Kondo, M.; Okubo, T.; Asami, A.; Noro, S.; Kitagawa, S.; Ishii, T.; Matsuzaka, H.; Seki, K. *Angew. Chem., Int. Ed.* **1999**, *38*, 140−143.
(13) Abrahams, B. F.; Jackson, P. A.; Robson, R. *Angew. Chem., Int. Ed.* **1998**, *37*, 2656−2659.
(14) Endo, K.; Koike, T.; Sawaki, T.; Hayashida, O.; Masuda, H.; Aoyama, H. *J. Am. Chem. Soc.* **1997**, *119*, 4117−4122.
(15) Sawaki, T.; Dewa, T.; Aoyama, Y. *J. Am. Chem. Soc.* **1998**, *120*, 8539−8540.

10.1021/cm990612m CCC: $19.00
Published on Web 04/07/2000

molecules, for instance, when immersed in the solvent. Despite the potential utility of these channel structures, most of crystalline coordination polymers are faced with a fragility of their porous structures upon the removal of guest molecules.[5,20,21,34] In other words, it has been impossible to create a porous function from coordination polymers which lose the crystallinity, undergo a phase change, or alter their morphology upon loss of their guest molecules.

Construction of robust channels is one of the intriguing challenges in the synthetic field of porous compounds. The "robustness" of compounds includes the properties that a channel or cavity could allow reversible release and adsorption of guests without the collapse of the porous structure. For the porous properties, it is of significance to build a well-associated network from metal−organic ligand systems. One synthetic approach for the purpose is to utilize a coordination bond for a three-dimensional link, for example, tongue-and-groove-type,[7,35,36] pillared-layer-type,[12] and cubic-type[37] coordination polymers have been synthesized, which retain the vacant channels even after removal of the guest molecules without structural change at ambient temperature. Similarly, hydrogen bonds to the coordination sheet have also been demonstrated to be useful.[10]

The other important synthetic approach is to use interpenetration.[26] Although many interpenetration structures have been reported to date, it has been considered that this type of structure is not consistent with the creation of porous structures because the cavities are usually occupied by the self-including

Scheme 1

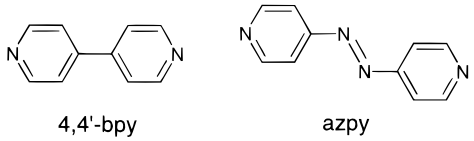

structure.[16−18,23−30] On this background, much attention has been paid to the inhibition of interpenetrated networks.[5,38,39] However, the interpenetration easily affords three dimensionally held networks, which could provide rigid structures. This is why we aimed at construction of a porous network with interpenetration, rather than prevent it, by using the 4,4′-azopyridine (azpy) ligand (Scheme 1), in which the longer metal−metal distance readily provides interpenetrated networks. Even if the interpenetration occurs, we could still expect the presence of voids for small-molecule inclusion when we used azpy. We have succeed in preparing new channel structures by interpenetrated networks of azpy ligand for adsorption of small molecules. The use of interpenetration is a new synthetic strategy for the creation of robust channel structures. We found that their porous three dimensionally held networks are so robust that methane molecules are adsorbed at ambient temperature. The methane adsorption property of the porous materials has attracted strong interest toward a development of a new natural gas storage method.[40−42] We present here the structures, stability, and gas adsorption properties of the porous compounds.

Experimental Section

Materials. $Mn(NO_3)_2 \cdot 6H_2O$, $Co(NO_3)_2 \cdot 6H_2O$, and $Cd(NO_3)_2 \cdot 4H_2O$ were obtained from Wako Co. $Co(NCS)_2 \cdot 4H_2O$ was obtained from Aldrich Chemical Co. Azpy was prepared according to the literature method.[46,47]

$[Mn(azpy)(NO_3)_2(H_2O)_2] \cdot 2EtOH$ (1·2EtOH). An ethanol solution (20 mL) of azpy (0.74 g, 4.0 mmol) was added to an acetone solution (20 mL) of $Mn(NO_3)_2 \cdot 6H_2O$ (0.57 g, 2.0 mmol). The solution was filtered and allowed to stand for 3 days at room temperature. Orange brick crystals were obtained in a few days. One of these crystals was used for X-ray crystallography. The residual crystals were collected by filtration, washed with ethanol, and dried under reduced pressure. The compound lost guest ethanol molecules during the drying process. The removal was monitored by IR spectroscopy. Yield: 0.31 g (0.78 mmol, 39%). Anal. Calcd for $C_{10}H_{12}MnN_6O_8$ (**1**): C, 30.09; H, 3.03; N, 21.05. Found: C, 29.11; H, 2.93; N, 21.05.

The X-ray crystal structure clearly demonstrates the porous structure of **1**·2EtOH. Although the dried compound **1** shows the sharp and intense diffraction lines for XRPD measurement,

(16) Hoskins, B. F.; Robson, R. *J. Am. Chem. Soc.* **1990**, *112*, 1546−1554.
(17) Robinson, F.; Zaworotko, M. J. *J. Chem. Soc., Chem. Commun.* **1995**, 2413−2414.
(18) Yaghi, O. M.; Li, H. *J. Am. Chem. Soc.* **1996**, *118*, 295−296.
(19) Zimmerman, S. C. *Science* **1997**, *276*, 543−544.
(20) Munakata, M.; Wu, L. P.; Kuroda-Sowa, T. *Bull. Chem. Soc. Jpn.* **1997**, *70*, 1727−1743.
(21) Kitagawa, S.; Kondo, M. *Bull. Chem. Soc. Jpn.* **1998**, *71*, 1739−1753.
(22) Yaghi, O. M.; Li, H.; Davis, C.; Richardson, D.; Groy, T. L. *Acc. Chem. Res.* **1998**, *31*, 474−484.
(23) Gable, R. W.; Hoskins, B. F.; Robson, R. *J. Chem. Soc., Chem. Commun.* **1990**, 1677−1678.
(24) MacGillivray, L. R.; Subramanian, S.; Zaworotko, M. J. *J. Chem. Soc., Chem. Commun.* **1994**, 1325−1326.
(25) Carlucci, L.; Ciani, G.; Proserpio, D. M.; Sironi, A. *J. Chem. Soc., Chem. Commun.* **1994**, 2755−2756.
(26) Yaghi, O. M.; Li, G. *Angew. Chem., Int. Ed. Engl.* **1995**, *34*, 207−209.
(27) Gardner, G. B.; Venkataraman, D.; Moore, J. S.; Lee, J. S. *Nature* **1995**, *374*, 792−795.
(28) Batten, S. R.; Hoskins, B. F.; Robson, R. *J. Am. Chem. Soc.* **1995**, *117*, 5385−5386.
(29) Carlucci, L.; Ciani, G.; Proserpio, D. M.; Sironi, A. *J. Am. Chem. Soc.* **1995**, *117*, 12861−12862.
(30) Hagrman, D.; Hammond, R. P.; Haushalter, R.; Zubieta, J. *Chem. Mater.* **1998**, *10*, 2091−2100.
(31) Yaghi, O. M.; Li, H. *J. Am. Chem. Soc.* **1995**, *117*, 10401−10402.
(32) Kawata, S.; Kitagawa, S.; Kumagai, H.; Ishiyama, T.; Honda, K.; Tobita, H.; Adachi, K.; Katada, M. *Chem. Mater.* **1998**, *10*, 3902−3912.
(33) Kawata, S.; Kitagawa, S.; Kumagai, H.; Kudo, C.; Kamesaki, H.; Ishiyama, T.; Suzuki, R.; Kondo, M.; Katada, M. *Inorg. Chem.* **1996**, *35*, 4449−4461.
(34) Li, H.; Davis, C. E.; Groy, T. L.; Kelley, D. G.; Yaghi, O. M. *J. Am. Chem. Soc.* **1998**, *120*, 2186−2187.
(35) Power, K. N.; Hennigar, T. L.; Zaworotko, M. J. *New. J. Chem.* **1998**, 177−181.
(36) Kepert, C. J.; Rosseinsky, M. J. *J. Chem. Soc. Commun.* **1999**, 375−376.
(37) Li, H.; Eddaoudi, M.; O′Keeffe, M.; Yaghi, O. M. *Nature* **1999**, *402*, 276−279.
(38) Zaworotko, M. J. *Angew. Chem., Int. Ed.* **1998**, *37*, 1211−1213.
(39) Reineke, T. M.; Eddaoudi, M.; Fehr, M.; Kelley, D.; Yaghi, O. M. *J. Am. Chem. Soc.* **1999**, *121*, 1651−1657.
(40) Mentasty, L.; Faccio, R. J.; Zgrablich, G. *Adsorpt. Sci. Technol.* **1991**, *8*, 105−113.
(41) Cracknell, R. F.; Gordon, P.; Gubbins, K. E. *J. Phys. Chem.* **1993**, *97*, 494−499.
(42) Mentasty, L.; Woestyn, A. M.; Zgrablich, G. *Adsorpt. Sci. Technol.* **1994**, *11*, 123−133.
(43) Zaworotko, M. J. *Chem. Soc. Rev.* **1994**, 283−288.
(44) Subramanian, S.; Zaworotko, M. J. *Angew. Chem., Int. Ed. Engl.* **1995**, *34*, 2127−2129.
(45) Brunet, P.; M.; S.; Wuest, J. D. *J. Am. Chem. Soc.* **1997**, *119*, 2737−2738.
(46) Brown, E. V.; Granneman, G. R. *J. Am. Chem. Soc.* **1975**, *97*, 621−627.
(47) Campbell, N.; Henderson, A. W.; Taylor, D. *J. Chem. Soc.* **1953**, 1281−2185.

Table 1. Crystallographic Data for $[Mn(azpy)(NO_3)_2(H_2O)_2]\cdot 2EtOH$ (1·2EtOH), $[Co_2(azpy)_3(NO_3)_4]\cdot Me_2CO\cdot 3H_2O$ (2·Me_2CO·3H_2O), $[Co(azpy)_2(NCS)_2]\cdot 0.5EtOH$ (3·0.5EtOH), $[Cd(azpy)_2(NO_3)_2]\cdot(azpy)$ (4·azpy), $[Cd_2(azpy)_3(NO_3)_4]\cdot 2Me_2CO$ (5·2Me_2CO)

compounds	**1**·2EtOH	**2**·$Me_2CO\cdot 3H_2O$	**3**·0.5EtOH	**4**·azpy	**5**·2Me_2CO
formula	$C_{14}H_{24}MnN_6O_{10}$	$C_{33}H_{36}Co_2N_{16}O_{16}$	$C_{23}H_{19}O_{0.5}N_{10}S_2Co$	$C_{30}H_{24}N_{14}CdO_6$	$C_{36}H_{36}N_{16}O_{14}Cd_2$
fw	490.31	1030.61	566.52	789.02	1141.60
lattice	monoclinic	tetragonal	orthorhombic	monoclinic	monoclinic
a, Å	24.488(4)	26.381(3)	18.066(4)	9.490(9)	21.954(5)
b, Å	11.868(3)		31.121(6)	27.405(6)	11.334(6)
c, Å	7.636(4)	13.318(7)	19.64(1)	13.584(7)	20.995(4)
β, deg	91.39(3)			109.44(5)	122.11(1)
V, Å^3	2218(1)	9268(2)	11039(6)	3331(3)	4425(2)
space group	*C*2/*c* (no.15)	$I4_1$ (no. 80)	*Ccca* (no. 68)	$P2_1/c$ (no. 14)	*C*2/*c* (no. 15)
Z	4	8	16	4	4
ρ(calcd) g cm^{-3}	1.471	1.477	1.363	1.573	1.713
F(000)	1016.00	4224.00	4640.00	1592.00	2288.00
μ(Mo Kα), cm^{-1}	6.56	7.99	8.06	7.23	10.47
diffractometer	AFC7R	AFC7R	AFC7R	AFC7R	AFC7R
radiation (λ, Å)	0.71069	0.71069	0.71069	0.71069	0.71069
T, °C	25	25	25	25	25
R_a	0.037	0.066	0.059	0.047	0.061
R_w[b]	0.038	0.061	0.068	0.045	0.073
no. of observns	2093($I > 3.00\sigma(I)$)	2501($I > 2.00\sigma(I)$)	3573($I > 3.00\sigma(I)$)	3699($I > 2.00\sigma(I)$)	3829($I > 3.00\sigma(I)$)
no. of variables	167	420	328	461	355

[a] $R = \sum||F_o| - |F_c||/\sum|F_o|$. [b] $R_w = [(\sum_w(|F_o| - |F_c|)^2/\sum_w F_o^2)]^{1/2}$.

their positions and pattern are not in agreement with the simulated pattern based on the single-crystal model without clathrate solvents. This means that the loss of the ethanol molecules of **1**·2EtOH causes phase transition or deformation of the structure. This is consistent with the negligible gas adsorption ability of this dried sample (vide infra).

$[Co_2(azpy)_3(NO_3)_4]\cdot Me_2CO\cdot 3H_2O$ (2·Me_2CO·3H_2O). An ethanol solution (5 mL) of azpy (0.18 g, 1.0 mmol) was carefully layered on top of an acetone solution (5 mL) of $Co(NO_3)_2\cdot 6H_2O$ (0.15 g, 0.5 mmol). Deep orange plate crystals began to form in a few days. One of these crystals was used for X-ray crystallography.

The bulk product was obtained by the addition of an ethanol solution (15 mL) of azpy (0.55 g, 3.0 mmol) into an acetone solution (15 mL) of $Co(NO_3)_2\cdot 6H_2O$ (0.44 g, 1.5 mmol). The obtained orange powder was collected by filtration, washed with ethanol, and dried under reduced pressure. The bulk compound lost acetone and a part of water guest molecules during the drying process. The removal was monitored by IR spectroscopy Yield: 0.64 g (0.67 mmol, 89%). Anal. Calcd for $C_{30}H_{28}Co_2N_{16}O_{14}$ (**2**·2H_2O): C, 37.75; H, 2.96; N, 23.48. Found: C, 37.70; H, 2.57; N, 22.97.

$[Co(azpy)_2(NCS)_2]\cdot 0.5EtOH$ (3·0.5EtOH). An ethanol solution (5 mL) of azpy (0.28 g, 1.5 mmol) was carefully layered on top of an aqueous solution (5 mL) containing $Co(NCS)_2\cdot 4H_2O$ (0.13 g, 0.5 mmol). Deep orange needle crystals began to form in a few days. One of these crystals was used for X-ray crystallography.

The bulk product was obtained by the addition of an ethanol solution (15 mL) of azpy (0.82 g, 4.5 mmol) into an aqueous solution (15 mL) containing $Co(NO_3)_2\cdot 6H_2O$ (0.38 g, 1.5 mmol). The obtained orange powder was collected by filtration, washed with ethanol, and dried under reduced pressure. Yield: 0.57 g (1.0 mmol, 67%). Anal. Calcd for $C_{23}H_{19}CoN_{10}O_{0.5}S_2$ (**3**·0.5EtOH): C, 48.76; H, 3.38; N, 24.72. Found: C, 49.29; H, 3.13; N, 24.96.

$[Cd(azpy)_2(NO_3)_2]\cdot(azpy)$ (4·azpy). An aqueous solution (15 mL) of $Cd(NO_3)_2\cdot 4H_2O$ (0.46 g, 1.5 mmol) was mixed with azpy (0.82 g, 4.5 mmol) in an ethanol (15 mL), and allowed to stand for 3 days at ambient temperature. The wine-red crystals obtained were collected by filtration, washed with ethanol, and dried under reduced pressure. Yield: 0.66 g (0.84 mmol, 56%) Anal. Calcd for $C_{30}H_{24}CdN_{14}O_6$: C, 45.67; H, 3.07; N, 24.85. Found: C, 45.55; H, 3.18; N, 24.73.

$[Cd_2(azpy)_3(NO_3)_4]\cdot 2Me_2CO$ (5·2Me_2CO). An ethanol solution (5 mL) of azpy (0.18 g, 1.0 mmol) was carefully layered on top of an acetone solution (5 mL) containing $Cd(NO_3)_2\cdot 4H_2O$ (0.15 g, 0.5 mmol). Deep orange plate crystals began to form in 1 month. One of these crystals was used for X-ray crystallography.

The bulk product was obtained by the addition of an ethanol solution (15 mL) of azpy (0.55 g, 3.0 mmol) into an acetone solution (15 mL) containing $Cd(NO_3)_2\cdot 4H_2O$ (0.46 g, 1.5 mmol). The obtained orange powder was collected by filtration, washed with ethanol, and dried under reduced pressure. During the drying process, the compound lost acetone guest molecules. The removal was monitored by IR spectroscopy. The obtained compound readily accommodated water molecules in the air.[48] Yield: 0.67 g (0.61 mmol, 81%). Anal. Calcd for $C_{30}H_{32}Cd_2N_{16}O_{16}$ (**5**·4H_2O): C, 32.83; H, 2.94; N, 20.42. Found: C, 32.74; H, 2.56; N, 20.74.

Physical Measurements. X-ray powder diffraction (XRPD) data were collected on a Rigaku RINT 2200Ultima diiffractometer by using Cu Kα radiation. Temperature control was achieved with a temperature control unit. The simulated powder patterns were obtained based on the coordinates upon removal of guest molecules from the single-crystal model. Thermal gravimetric (TG) analyses were carried out with a Seiko Instruments SSC5200 in a nitrogen atmosphere (heating rate: 5 K/min).

X-ray Structure Determination. For each compound, a suitable crystal was sealed in a glass capillary. Data collections were carried out on a Rigaku AFC7R automated diffractometer fitted with a monochromatic Mo Kα radiation source (λ = 0.71069 Å). Unit cell constants were obtained from a least-squares refinement using the setting angles of 25 well-centered reflections in the ranges $40.28 < 2\theta < 46.60°$ for **1**·2EtOH, $25.07 < 2\theta < 28.29°$ for **2**·$Me_2CO\cdot 3H_2O$, $6.75 < 2\theta < 13.50°$ for **3**·0.5EtOH, $6.74 < 2\theta < 12.85°$ for **4**·azpy, and $29.65 < 2\theta < 30.04°$ for **5**·2Me_2CO. Crystallographic data are given in Table 1. An empirical absorption correction based on azimuthal scans of several reflections was applied. The data were corrected for Lorentz and polarization effects. The structures were solved by direct methods, and refined anisotropically for all non-hydrogen atoms by full-matrix least-squares technique. In the case of **2**·$Me_2CO\cdot 3H_2O$, the structure was refined anisotropically for cobalt, nitrogen, and oxygen atoms, and refined isotropically for all carbon atoms. The hydrogen atoms, H(1)−H(6) of **1**·2EtOH and H(1)−H(12) of **5**·2Me_2CO, were refined isotropically. Other hydrogen atoms of each compound were placed in idealized positions, and were included but not refined. All calculations were performed using the TEXSAN crystallographic software package of Molecular Structure Corporation.

Gas Adsorption Measurements. The adsorption isotherms of methane gas were measured according to the re-

(48) Similar replacement of the organic molecules with water molecules was reported in $[Ag(hat)ClO_4]\cdot 2CH_3NO_2$ (hat = 1,4,5,8,9,12-hexaazatriphenylene).[13]

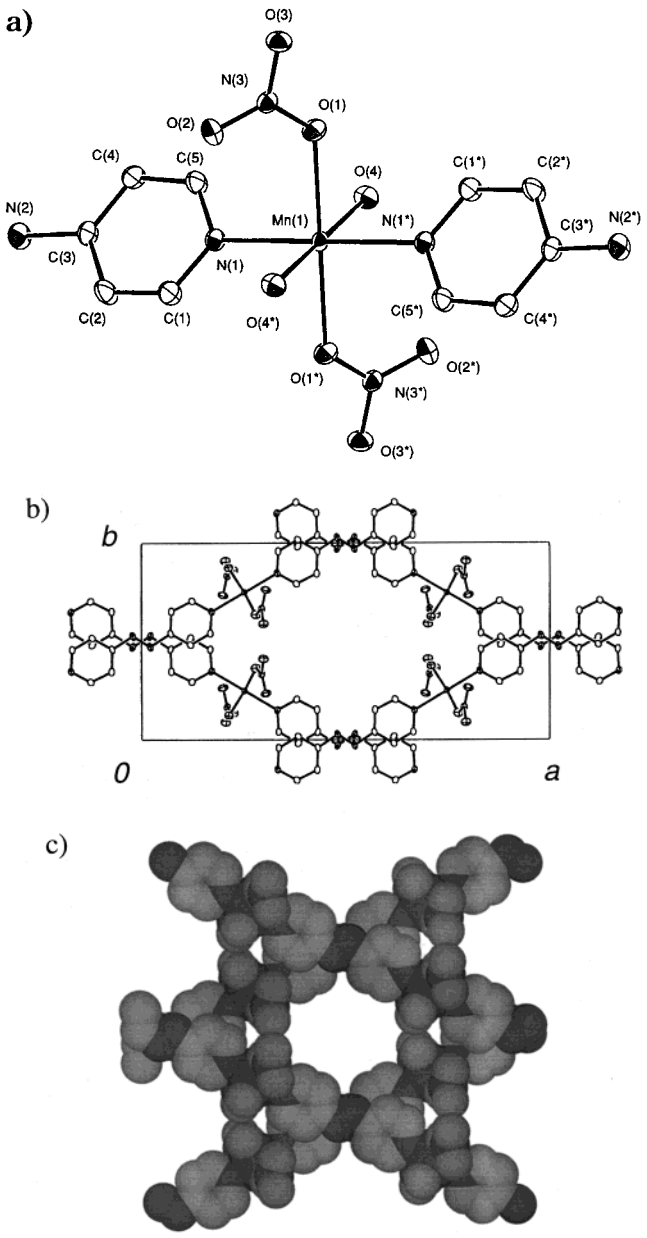

Figure 1. (a) ORTEP drawing of the manganese center of **1**·2EtOH with the non-hydrogen atoms at the 30% probability level; (b) projection of $[Mn(azpy)(NO_3)_2(H_2O)_2]_n$ chains of **1**·2EtOH with the non-hydrogen atoms along the *c* axis; and (c) a space-filling model of a *logcabin* structure of **1**·2EtOH with the non-hydrogen atoms along the *c* axis, indicating the aspects of large channel structure. The ethanol molecules are omitted for clarity.

ported procedure.[49,50] The apparatus was equipped with a Cahn R-100 electrobalance contained within a SUS steel pressure chamber which was connected with two separate lines for evacuation and adsorbate gas pressurization. After the each sample was set in the apparatus, the guest molecules in the channels were removed under reduced pressure at 25 °C until no further weight loss was observed. The removal process was monitored by the change of the weight, in which the weight lost was corresponding to that of the guest molecules estimated from the TG data. The methane gas was dosed into the adsorption chamber, and then the change of the weight of the sample was monitored. The entire adsorption isotherms at 25 °C were determined by increasing the adsorbate gas pressure to a maximum of 36 atm. After the buoyancy was corrected to the obtained amount of the weight change, the adsorbed amount was calculated.

(49) Zhang, S.-Y.; Talu, O.; Hayhurst, D. T. *J. Phys. Chem.* **1991**, *95*, 1722−1726.
(50) Zuech, J. L.; Hines, A. L.; Sloan, E. D. *Ind. Eng. Chem. Process Des. Dev.* **1983**, *22*, 172−174.

Scheme 2

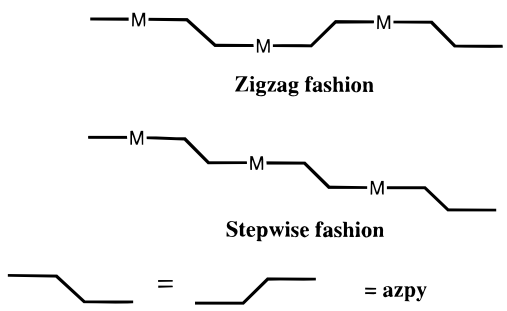

Scheme 3

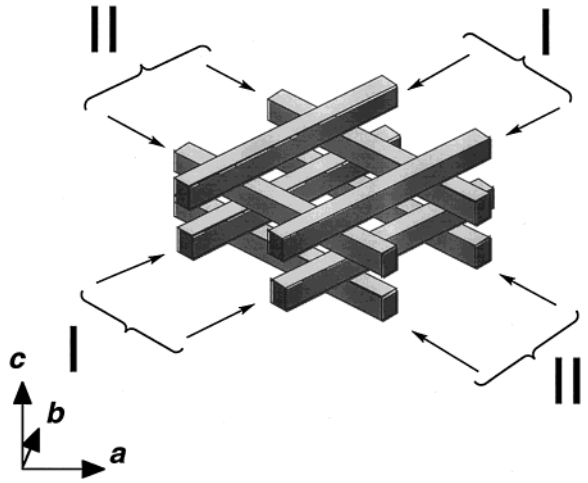

Results and Discussion

Crystal Structure of 1·2EtOH. An ORTEP view of the manganese center of this compound is shown in Figure 1a with numbering scheme, where the metal sits on the crystallographic inversion center. The selected bond distances and angles with their estimated standard deviations are listed in Table 2. The manganese center is based on a distorted octahedral environment with two pyridine nitrogen donors, two nitrate oxygen donors, and two water molecules, in which each ligand occupies the trans position. The nitrate anions ligate to the manganese atom as a monodentate fashion. In the coordination octahedron, all the *trans*-L−Mn−L bond angles are crystallographically linear, and all the *cis*-L−Mn−L angles are slightly deviated from 90° (81−99°).

Each azpy ligand links two manganese centers (Mn···Mn; 13.6 Å) to form an infinite one-dimensional chain in the *ab* plane (Figure 1b). The two pyridine rings of the azpy ligand are almost coplanar and parallel to the *ab* plane. The mode of the chains is not a zigzag fashion but stepwise one (Scheme 2). The *trans*-O(1)−Mn(1)−O(1*) and *trans*-O(4)−Mn(1)−O(4*) vectors bend by 36.6° and 45.3° to the *ab* plane, respectively. As shown in Scheme 3, the chains, oriented at the angle of 26° to the *a* axis, form a flat parallel array I, while the other neighboring array II exists, whose chains are oriented by −26° to the *a* axis.

Table 2. Selected Bond Distances (Å) and Angles (deg)

$[Mn(azpy)(NO_3)_2(H_2O)_2]\cdot 2EtOH$ (**1**·2EtOH)[a]

Distances

Mn(1)−O(1)	2.207(2)	Mn(1)−O(4)	2.151(2)	Mn(1)−N(1)	2.291(2)		

Angles

O(1)−Mn(1)−O(1*)	180.0	O(1)−Mn(1)−O(4)	81.80(8)	O(1)−Mn(1)−O(4*)	98.20(8)	O(1)−Mn(1)−N(1)	94.04(7)
O(1)−Mn(1)−N(1*)	85.96(7)	O(1*)−Mn(1)−N(1)	85.96(7)	O(4)−Mn(1)−O(4*)	180.0	O(4)−Mn(1)−N(1)	87.70(8)
O(4)−Mn(1)−N(1*)	92.30(8)	N(1)−Mn(1)−N(1*)	180.0				

$[Co_2(azpy)_3(NO_3)_4]\cdot Me_2CO\cdot 3H_2O$ (**2**·Me_2CO·$3H_2O$)[b]

Distances

Co(1)−O(1)	2.20(1)	Co(1)−O(2)	2.36(1)	Co(1)−O(4)	2.17(1)	Co(1)−O(5)	2.41(1)
Co(1)−N(1)	2.124(9)	Co(1)−N(5)	2.158(8)	Co(1)−N(9)	2.15(1)	Co(2)−O(7)	2.20(1)
Co(2)−O(8)	2.63(1)	Co(2)−O(10)	2.15(1)	Co(2)−O(11)	2.17(1)	Co(2)−N(2)	2.173(8)
Co(2)−N(6*)	2.150(9)	Co(2)−N(11)	2.18(1)				

Angles

O(1)−Co(1)−O(2)	56.0(4)	O(1)−Co(1)−O(4)	173.1(4)	O(1)−Co(1)−O(5)	132.0(4)	O(1)−Co(1)−N(1)	86.1(4)
O(1)−Co(1)−N(5)	87.5(4)	O(1)−Co(1)−N(9)	87.6(4)	O(2)−Co(1)−O(4)	130.6(4)	O(2)−Co(1)−O(5)	76.6(4)
O(2)−Co(1)−N(1)	86.8(4)	O(2)−Co(1)−N(5)	80.4(4)	O(2)−Co(1)−N(9)	143.0(4)	O(4)−Co(1)−O(5)	54.8(4)
O(4)−Co(1)−N(1)	96.0(4)	O(4)−Co(1)−N(5)	91.6(4)	O(4)−Co(1)−N(9)	85.7(4)	O(5)−Co(1)−N(1)	84.5(3)
O(5)−Co(1)−N(5)	91.5(4)	O(5)−Co(1)−N(9)	140.3(4)	N(1)−Co(1)−N(5)	167.2(4)	N(1)−Co(1)−N(9)	97.8(4)
N(5)−Co(1)−N(9)	93.1(4)	O(7)−Co(2)−O(8)	51.0(4)	O(7)−Co(2)−O(10)	173.9(4)	O(7)−Co(2)−O(11)	127.1(4)
O(7)−Co(2)−N(2)	88.8(4)	O(7)−Co(2)−N(6*)	90.1(4)	O(7)−Co(2)−N(11)	86.5(4)	O(8)−Co(2)−O(10)	133.7(4)
O(8)−Co(2)−O(11)	76.1(4)	O(8)−Co(2)−N(2)	85.9(4)	O(8)−Co(2)−N(6*)	87.1(4)	O(8)−Co(2)−N(11)	137.5(4)
O(10)−Co(2)−O(11)	57.7(4)	O(10)−Co(2)−N(2)	87.8(4)	O(10)−Co(2)−N(6*)	94.0(4)	O(10)−Co(2)−N(11)	88.8(4)
O(11)−Co(2)−N(2)	85.1(4)	O(11)−Co(2)−N(6*)	89.3(4)	O(11)−Co(2)−N(11)	146.4(5)	N(2)−Co(2)−N(6*)	171.9(4)
N(2)−Co(2)−N(11)	96.7(4)	N(6*)−Co(2)−N(11)	91.2(4)				

$[Co(azpy)_2(NCS)_2]\cdot 0.5EtOH$ (**3**·0.5EtOH)[c]

Distances

Co(1)−N(1)	2.165(4)	Co(1)−N(5)	2.166(4)	Co(1)−N(9)	2.094(5)	Co(2)−N(2)	2.181(4)
Co(2)−N(6)	2.185(4)	Co(2)−N(10)	2.065(4)				

Angles

N(1)−Co(1)−N(1*)	92.6(2)	N(1)−Co(1)−N(5)	178.8(2)	N(1)−Co(1)−N(5*)	88.6(1)	N(1)−Co(1)−N(9)	89.3(2)
N(1)−Co(1)−N(9*)	88.9(2)	N(5)−Co(1)−N(5*)	90.2(2)	N(5)−Co(1)−N(9)	90.5(2)	N(5)−Co(1)−N(9*)	91.4(2)
N(5)−Co(1)−N(9*)	90.5(2)	N(9)−Co(1)−N(9*)	177.4(3)	N(2)−Co(2)−N(2*)	86.9(2)	N(2)−Co(2)−N(6)	177.1(2)
N(2)−Co(2)−N(6*)	92.3(1)	N(2)−Co(2)−N(10)	91.7(2)	N(2)−Co(2)−N(10*)	89.8(2)	N(2*)−Co(2)−N(6*)	177.1(2)
N(6)−Co(2)−N(6*)	88.6(2)	N(6)−Co(2)−N(10)	91.1(2)	N(6)−Co(2)−N(10*)	87.5(2)	N(10)−Co(2)−N(10*)	178.0(2)
Co(1)−N(9)−C(21)	150.9(4)	Co(2)−N(10)−C(22)	158.4(4)				

$[Cd(azpy)_2(NO_3)_2]\cdot$(azpy) (**4**·azpy)

Distances

Cd(1)−O(1)	2.348(4)	Cd(1)−O(4)	2.422(6)	Cd(1)−O(5)	2.693(9)	Cd(1)−N(1)	2.390(4)
Cd(1)−N(3)	2.367(4)	Cd(1)−N(5)	2.378(4)	Cd(1)−N(7)	2.357(4)		

Angles

O(1)−Cd(1)−O(4)	168.6(2)	O(1)−Cd(1)−O(5)	148.5(2)	O(1)−Cd(1)−N(1)	87.9(1)	O(1)−Cd(1)−N(3)	91.2(1)
O(1)−Cd(1)−N(5)	78.7(2)	O(1)−Cd(1)−N(7)	89.4(2)	O(4)−Cd(1)−O(5)	42.9(2)	O(4)−Cd(1)−N(1)	89.4(2)
O(4)−Cd(1)−N(3)	90.8(2)	O(4)−Cd(1)−N(5)	112.5(2)	O(4)−Cd(1)−N(7)	79.3(2)	O(5)−Cd(1)−N(1)	95.0(2)
O(5)−Cd(1)−N(3)	87.8(2)	O(5)−Cd(1)−N(5)	69.9(2)	O(5)−Cd(1)−N(7)	122.1(2)	N(1)−Cd(1)−N(3)	175.9(2)
N(1)−Cd(1)−N(5)	91.3(1)	N(1)−Cd(1)−N(7)	86.5(1)	N(3)−Cd(1)−N(5)	92.4(2)	N(3)−Cd(1)−N(7)	89.5(2)
N(5)−Cd(1)−N(7)	168.0(1)						

$[Cd_2(azpy)_3(NO_3)_4]\cdot 2Me_2CO$ (**5**·$2Me_2CO$)

Distances

Cd(1)−O(1)	2.399(5)	Cd(1)−O(2)	2.523(4)	Cd(1)−O(4)	2.390(4)	Cd(1)−O(5)	2.463(5)
Cd(1)−N(1)	2.328(5)	Cd(1)−N(3)	2.333(5)	Cd(1)−N(5)	2.347(5)		

Angles

O(1)−Cd(1)−O(2)	51.8(2)	O(1)−Cd(1)−O(4)	137.6(2)	O(1)−Cd(1)−O(5)	170.4(2)	O(1)−Cd(1)−N(1)	92.1(2)
O(1)−Cd(1)−N(3)	83.5(2)	O(1)−Cd(1)−N(5)	87.2(2)	O(2)−Cd(1)−O(4)	85.9(2)	O(2)−Cd(1)−O(5)	137.7(2)
O(2)−Cd(1)−N(1)	85.7(2)	O(2)−Cd(1)−N(3)	79.1(2)	O(2)−Cd(1)−N(5)	139.0(2)	O(4)−Cd(1)−O(5)	51.8(2)
O(4)−Cd(1)−N(1)	86.9(2)	O(4)−Cd(1)−N(3)	85.9(2)	O(4)−Cd(1)−N(5)	135.1(2)	O(5)−Cd(1)−N(1)	90.4(2)
O(5)−Cd(1)−N(3)	96.6(2)	O(5)−Cd(1)−N(5)	83.3(2)	N(1)−Cd(1)−N(3)	163.6(2)	N(1)−Cd(1)−N(5)	96.9(2)
N(3)−Cd(1)−N(5)	98.6(2)						

[a–c] Symmetry codes: *a*, (*) $-x, y + 1, {}^3/_2 - z$. *b*, (*) $x, y - 1, z$. *c*, (*) $-x, -y, -z + 1$.

The chains of the arrays I and II are linked by hydrogen bonds between the terminal oxygen atoms of the coordinating nitrate and water molecules (N···O = 2.7 and 3.2 Å), resulting in formation of a three-dimensional network, which is described as a *logcabin* structure (Scheme 3). This framework creates hydrophobic large channels along the *c* axis with dimensions of about 8 × 8 Å (Figure 1c),[51] which are filled with two ethanol molecules per manganese atom. The two ethanol molecules are hydrogen bonded to form a dimer structure. In addition, the dimer units are connected by hydrogen bondings to give a one-dimensional chain

(51) Hereafter the channel dimensions are estimated from the van der Waals radii for carbon (1.70 Å), nitrogen (1.55 Å), oxygen (1.40 Å), and sulfur (1.80 Å).

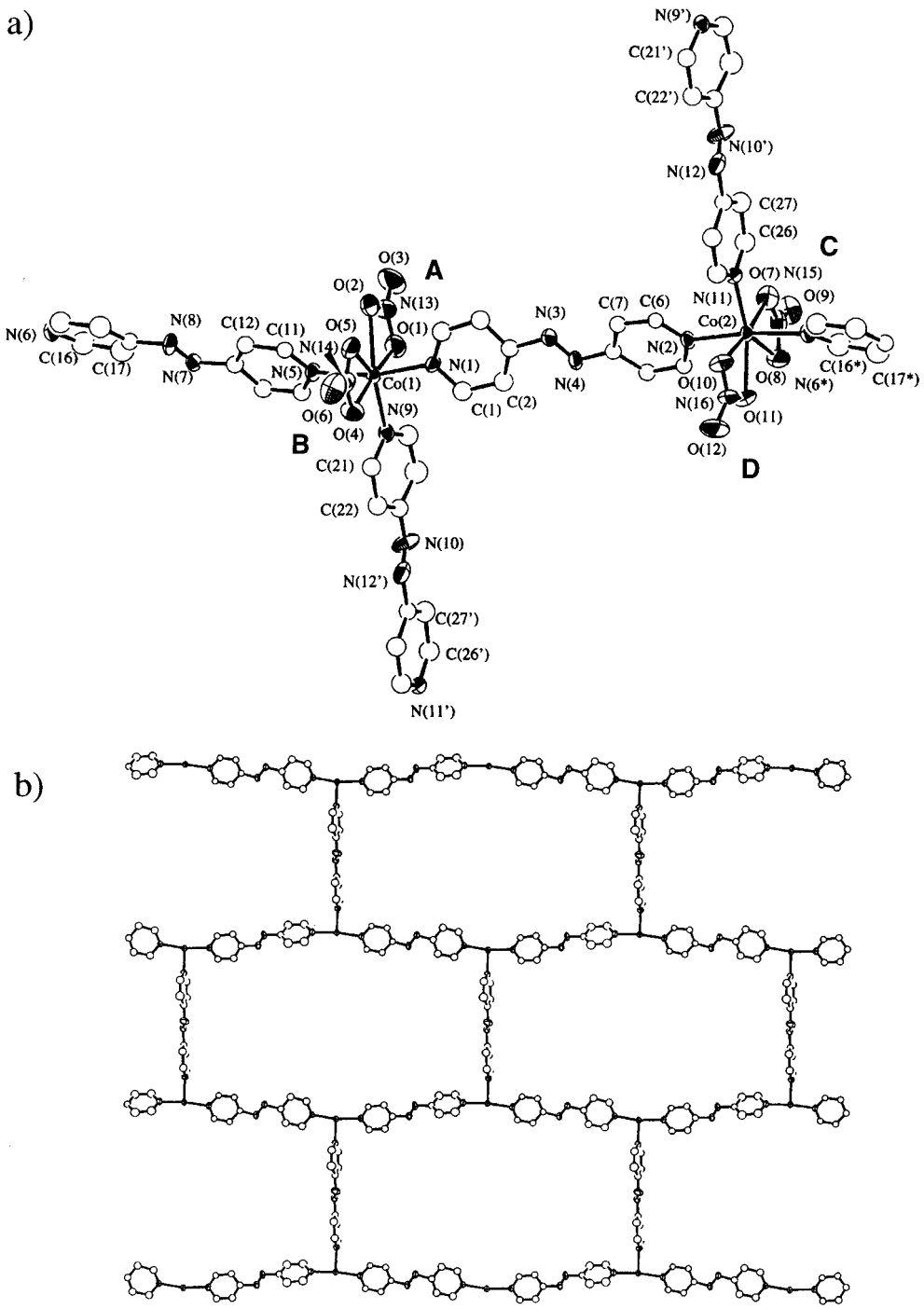

Figure 2. (a) ORTEP view of cobalt centers of **2**·Me_2CO·$3H_2O$ with non-hydrogen atoms at the 30% probability level. The numbers of unlabeled pyridine carbon atoms follow from those given. (b) View of the *brick-wall*-type network of **2**·Me_2CO·$3H_2O$ with non-hydrogen atoms. The nitrate anions are omitted for clarity.

in the channel. These guest ethanol molecules are not hydrogen bonded to the channel wall. Similarly, the compounds, **2**·Me_2CO·$3H_2O$, **3**·0.5EtOH, and **5**·$2Me_2CO$ include guest solvent molecules in the channels (vide infra). Each clathrate molecule also reveals no hydrogen-bonding interaction with the channel framework.

Crystal Structure of 2·Me_2CO·$3H_2O$. Figure 2a shows the local coordination environment of the cobalt centers. Crystallographically independent two cobalt centers are linked by an azpy ligand. Two types of coordination modes are observed in the four nitrate anions which associate with the two cobalt atoms. A nitrate has been assigned to three binding modes by the coordination geometries, i.e., (i) bidentate, (ii) anisobidentate, and (iii) unidentate.[52] On the basis of these criteria, one nitrate ligand D (defined in the Figure 2a) is assigned to the anisobidentate, while others A−C are the bidentate. As a result, geometries of the both two cobalt centers are regarded as a pentagonal bipyramid.

As far as the pyridyl groups are concerned, a T-shaped module is recognized, which have been found in several

(52) Dowling, C.; Murphy, V. J.; Parkin, G. *Inorg. Chem.* **1996**, *35*, 2415−2420.

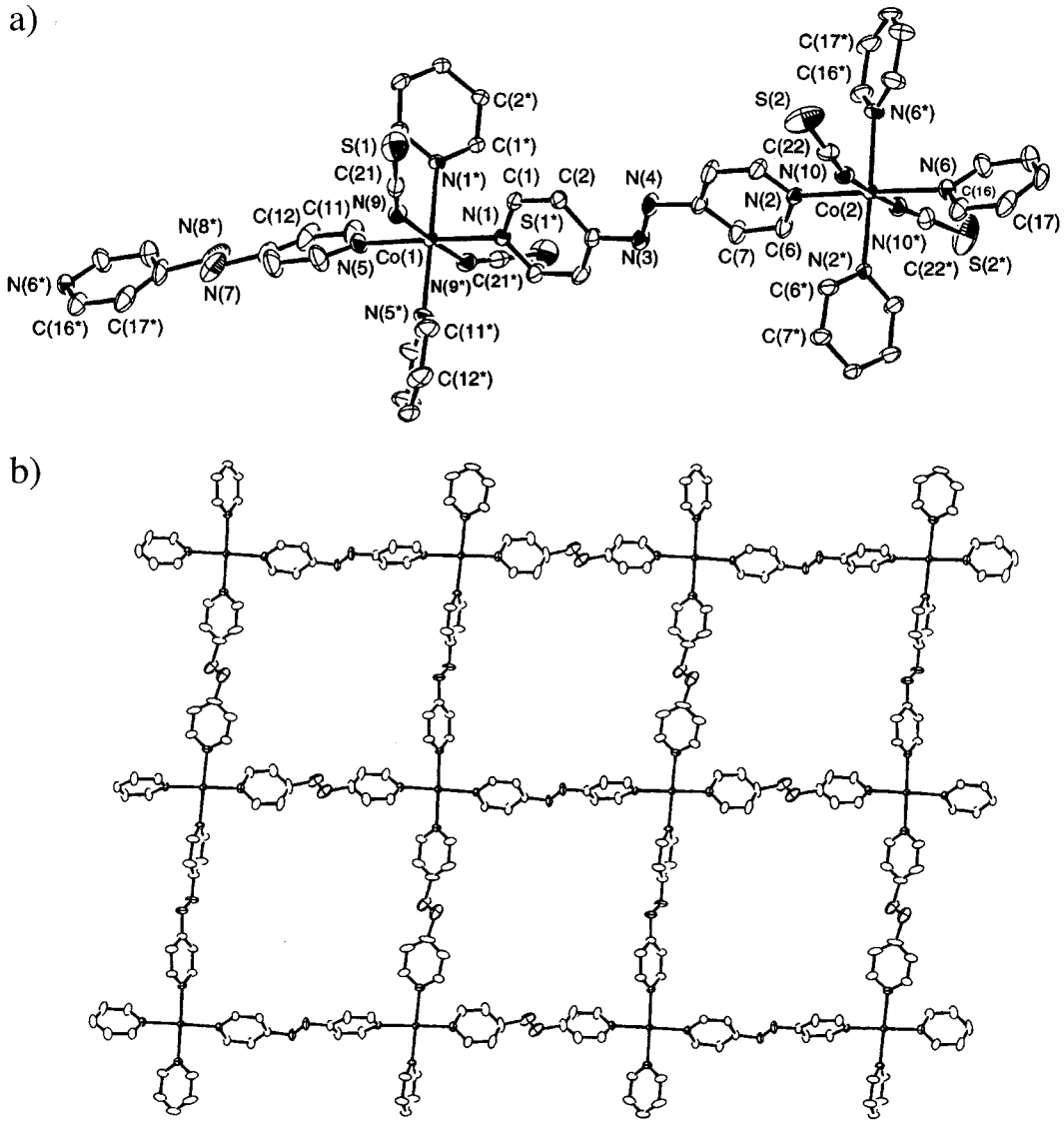

Figure 3. (a) ORTEP view of cobalt centers of **3**·0.5EtOH at the 30% probability level. The hydrogen atoms are omitted for clarity. The numbers of unlabeled pyridine carbon atoms follow from those given. (b) View of the two-dimensional sheet structure of **3**·0.5EtOH. The hydrogen atoms and isothiocyanate anions are omitted for clarity.

coordination polymers.[7,35,53−57] An assembly of the T-shaped module builds a *brick-wall*-type two-dimensional network of **2** (Figure 2b). The network is also considered to be constructed from chains with a stepwise fashion (Scheme 2) and azpy ligands as interchain linkers. The pyridine rings of the azpy in the chain are parallel to the sheet, while those connecting the chains are perpendicular to the sheet (Figure 2b). These sheets are quadruply interpenetrated. Although the large pores (about 24 × 11 Å) of each sheet are filled due to the mutual interpenetration, small size of channels (about 4 × 3 Å) are recognized, filled with clathrate acetone and water molecules at this moment. Each clathrate molecule is not held in the cavities by hydrogen bonding interactions but van der Waals interactions with the channel wall. Holding of clathrate molecules by only van der Waals interactions is also observed in the channel cavities of other interpenetrated networks, **3** and **5**.

Crystal Structure of 3·0.5EtOH. Figure 3a shows an ORTEP view of crystallographically independent two cobalt centers of **3**·0.5EtOH. Each cobalt center has a distorted octahedral geometry with four pyridine nitrogen atoms and two trans thiocyanato nitrogen atoms. The four pyridine units coordinated to the cobalt atom are arranged in a propeller fashion. The Co−N (pyridine) distances (av 2.174 (4) Å) are longer than those of Co−N (NCS) (av 2.080 (5) Å). The Co−N−C bonds formed by the NCS^- ligands show the bending angle of 154.7° (average).

Each cobalt center is linked by azpy to yield a *rhombus*-type two-dimensional network with the corner angles of about 95° and 85° (Figure 3b). The network is also considered to be constructed from chains with a stepwise mode (Scheme 2). The sheet, which has large

(53) Fujita, M.; Kwon, Y. J.; Sasaki, O.; Yamaguchi, K.; Ogura, K. *J. Am. Chem. Soc.* **1995**, *117*, 7287−7288.
(54) Losier, P.; Zaworotko, M. J. *Angew. Chem., Int. Ed. Engl.* **1996**, *35*, 2779−2782.
(55) Hennigar, T. L.; MacQuarrie, D. C.; Losier, P.; Rogers, R. D.; Zaworotko, M. J. *Angew. Chem., Int. Ed. Engl.* **1997**, *36*, 972−973.
(56) Fujita, M.; Aoyagi, M.; Ogura, K. *Bull. Chem. Soc. Jpn.* **1998**, *71*, 1799−1804.
(57) Kondo, M.; Asami, A.; Fujimoto, K.; Noro, S.; Kitagawa, S.; Ishii, T.; Matsuzaka, H. *J. Inorg. Mat.* **1999**, *1*, 73−75.

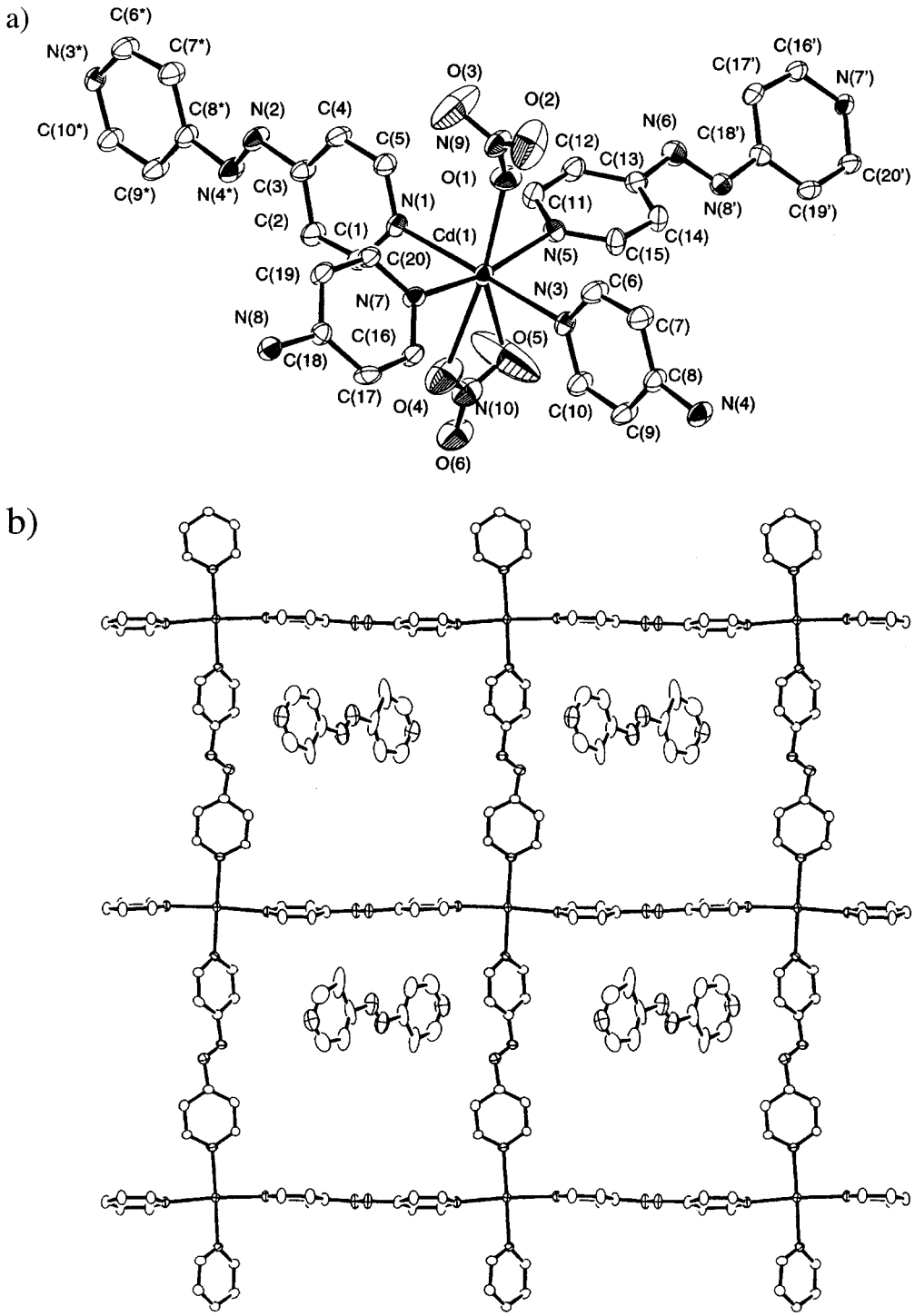

Figure 4. (a) ORTEP view of cadmium center of **4**·azpy. The hydrogen atoms are omitted for clarity and (b) view of the two-dimensional sheet structure of **4**·azpy including free azpy in the cavities. The hydrogen atoms and nitrate anions are omitted for clarity.

pores (about 10 × 10 Å), encounters double-interpenetration, giving rise to a tightly held three-dimensional structure. Despite the interpenetration, this network creates channels with dimensions of about 3 × 3 Å, which include an ethanol molecule per two cobalt atoms.

Crystal Structure of 4·azpy. Figure 4a shows an ORTEP drawing around a cadmium center of **4**·azpy. The four nitrogen atoms of bridging azpy and three oxygen atoms of the two nitrate anions are coordinated to the cadmium atom, resulting in a heptacoordinated cadmium center, which has two nitrate anions in unidentate and bidentate fashions.

Each cadmium center is linked by azpy to form a *square-grid*-type two-dimensional network (Figure 4b), forming square cavities of about 11 × 11 Å, in which the Cd(azpy) chains along the *b* axis show the zigzag fashion, and the other chains along the $(a + c)$ vector exhibit the stepwise one (Scheme 2). The pyridine rings of the azpy ligand along the $(a + c)$ vector are coplanar; the dihedral angle of the two pyridine rings linked by azo group is about 8.0°. On the other hand, the two pyridine rings along the *b* axis show a large deviation from a planarity with the dihedral angle of 45.0°.

The two-dimensional layers of **4**·azpy stack without interpenetration to provide large channels (about 7 × 4 Å) along the *c* axis. These channels are filled with free azpy molecules, indicative of no space for other guest molecules. The guest azpy molecule is associated with a template for the cavity formation in the assembling process. These guest molecules are not easily removed under reduced pressure, or immersed in the organic solvents such as benzene, toluene, acetonitrile, alcohol, or hexane.

Crystal Structure of 5·2Me$_2$CO. An ORTEP drawing of the structure around the cadmium atom in **5**·2Me$_2$CO is shown in Figure 5a with numbering scheme. The cadmium has a distorted pentagonal-bipyramidal geometry with three pyridyl nitrogen atoms and four oxygen atoms of two bidentate nitrate anions. A T-shaped module is recognized from the geometry. The two pyridine rings of the azpy B (see in Figure 5a) are nearly coplanar, while the two pyridine rings of the azpy A is not coplanar with dihedral angle of 65.1°.

The assembly of the T-shaped module forms a *herringbone*-type two-dimensional network in the *bc* plane (Figure 5b), which is comprised of rectangular large cavities with the dimensions of about 23 × 11 Å. The unique feature of this sheet is a large undulation (Figure 5c(i)). The period and the thickness of the undulated sheet are about 34 and 11 Å, respectively. These sheets are triply interpenetrated and are schematically illustrated in Figure 5c. Despite the interpenetration, there are still large channels (about 5 × 5 Å) through the sheets, which include acetone molecules. The channel structure is shown in Figure 5d.

It should be emphasized that **4**·azpy and **5**·2Me$_2$CO are obtained from the different solvent systems, ethanol/H$_2$O and ethanol/acetone, respectively. The channel of **4**·azpy accommodates free azpy ligands, whereas that of **5**·2Me$_2$CO accommodates acetone molecules; the selective formations of the two crystal compounds are controlled by the solvent system. The similar compounds having the herringbone structure were isolated from CH$_2$Cl$_2$.[58,59] The channel sizes of these interpenetrated networks, **2**, **3**, and **5** are not so large for the formation of further interpenetration. In other words, each interpenetrated network could be maximum.

Network Motifs Constructed from the Azpy Ligand. We can summarize crystal structures obtained in this work. Scheme 4 illustrates a variety of coordination networks, *chain* (**1**·2EtOH), *brick-wall* (**2**·Me$_2$CO·3H$_2$O), *rhombus-grid* (**3**·0.5EtOH), *square-grid* (**4**·azpy), and *herringbone* (**5**·2Me$_2$CO) motifs. The 4,4′-bipyridine (4,4′-bpy) has been extensively used for the construction of self-assembled networks.[1,21,23,35,60−63] Despite the numerous synthetic studies, there have been no examples of *brick-wall*- and *herringbone*-type networks with 4,4′-bpy. This result demonstrates a rich coordination polymer chemistry of the azpy ligand.

Scheme 4

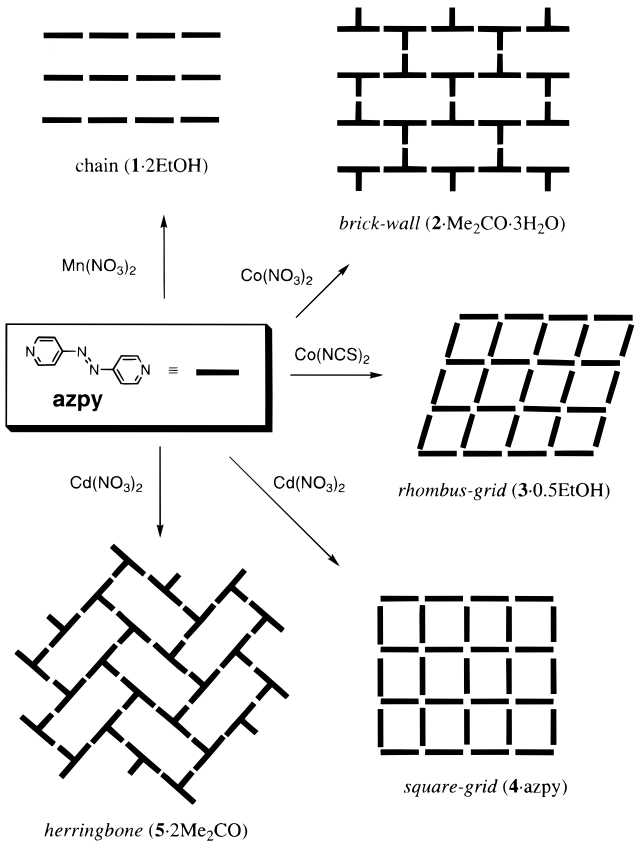

Scheme 5

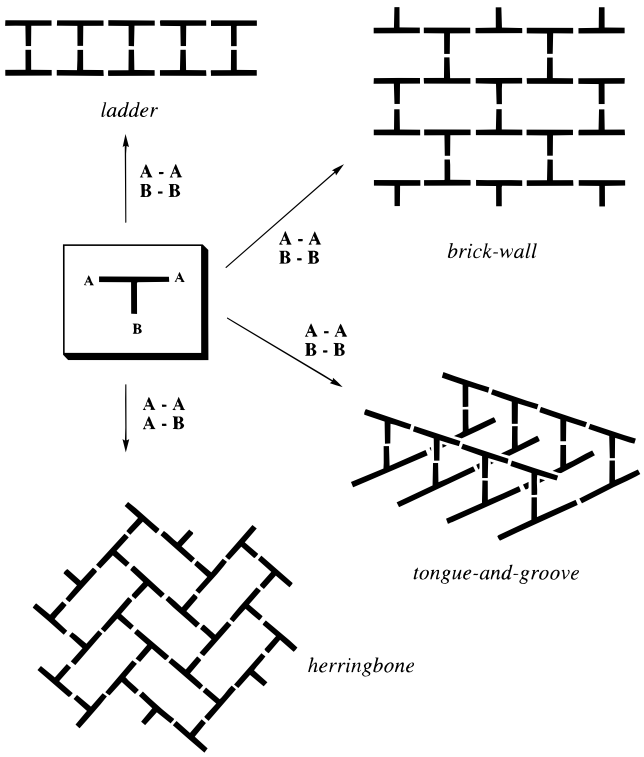

These networks are found to be constructed from linear, T-shaped, and cross-shaped modules. Among these modules, the T-shaped-type could provide a vari-

(58) Withersby, M. A.; Blake, A. J.; Champness, N. R.; Cooke, P. A.; Hubberstey, P.; Schröder, M. *New. J. Chem.* **1999**, *23*, 573−575.
(59) Carlucci, L.; Ciani, G.; Proserpio, D. M. *J. Chem. Soc., Dalton Trans.* **1999**, 1799−1804.
(60) Withersby, M. A.; Blake, A. J.; Champness, N. R.; Hubberstey, P.; Li, W.-S.; Schröder, M. *Angew. Chem., Int. Ed. Engl.* **1997**, *36*, 2327−2329.
(61) Huang, S. D.; Xiong, R.-G. *Polyhedron* **1997**, *16*, 3929−3939.
(62) Lu, J.; Paliwala, T.; Lim, S. C.; Yu, C.; Niu, T.; Jacobson, A. J. *Inorg. Chem.* **1997**, *36*, 923−929.
(63) MacGillivray, L. R.; Groeneman, R. H.; Atwood, J. L. *J. Am. Chem. Soc.* **1998**, *120*, 2676−2677.

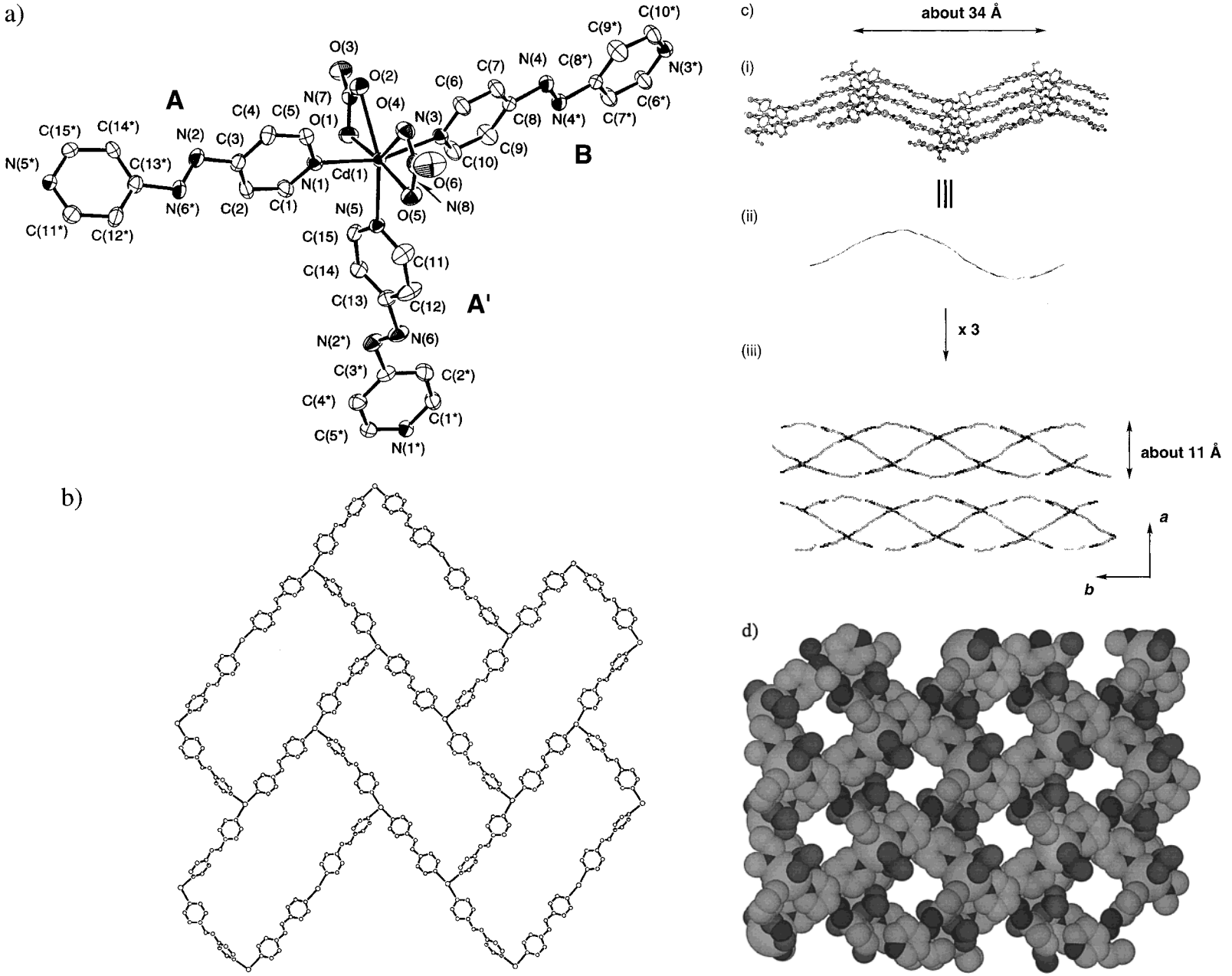

Figure 5. (a) ORTEP view of cadmium center of **5**·2Me_2CO. (b) The *herringbone* two-dimensional sheet of **5**·2Me_2CO. The coordinated nitrate anions and clathrate acetone molecules are omitted for clarity. (c) (i) The side view of the sheet projected down the *c* axis direction. (ii) The sheet is drawn as a simple undulating motif. (iii) The three motifs interpenetrate mutually to afford a layer. (d) The cross section of the channels by van der Waals radii model. Channels are created through microcavities of the layers.

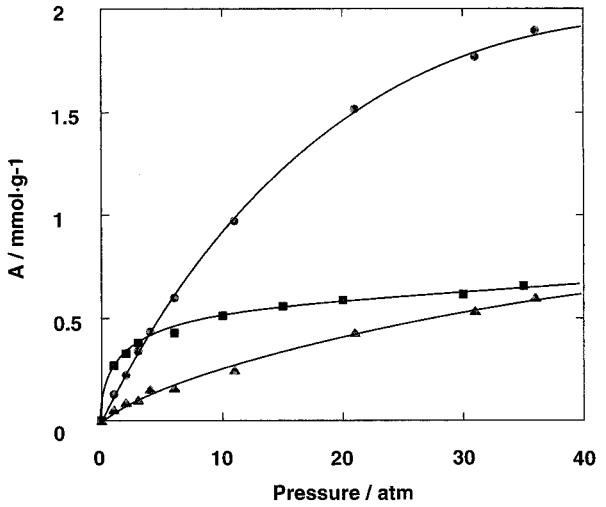

Figure 6. Isotherms for the adsorption of methane on **2** (▲), **3** (■), and **5** (●) at 298 K in the range of 1−36 atm; A = absolute adsorption in mmol of adsorbed methane per gram of anhydrous sample.

ety of networks, *ladder*,[53,54] *brick-wall*,[53,64] and *tongue-and-groove*[7,35] as shown in Scheme 5. Interestingly, these frameworks are easily obtained by the combination of the terminal ends of T-shaped module. For instance, the *herringbone*-type network is built up by not only A−A but also the A−B links. This A−B-type linkage is the first example of the assembled networks of the T-shaped modules.

Gas Adsorption Properties. To evaluate the framework rigidity of these porous compounds, the methane adsorption property of their dried samples were measured at ambient temperature. Figure 6 shows the isotherms of methane adsorption of these three compounds in the pressure range between 1 and 36 atm at 298 K. The high-pressure adsorption of supercritical methane in the micropore field has been studied with the following extended Dubinin−Radushkevich (DR) equation:[65,66]

$$[\ln(W_L/W)]^{1/2} = (RT/\beta E_0)(\ln P_{0q} - \ln P) \qquad (1)$$

Here the parameters, W, βE_0, and P_{0q} are the amount of adsorption at a pressure P, the adsorption energy, and the saturated vapor pressure of the quasi-vaporized supercritical methane, respectively. The inherent micropore volume, W_L, is determined by the Langmuir plot.[65,66] The isotherms of **3** and **5**, which are well explained by this equation, are consistent with those of the micropore-filling mechanism.[65,66] The adsorption ability of **5** is comparable to that of zeolite 13 X (about 1.8 mmol at 36 atm).[21] The obtained parameters, W_L (mmol g^{-1}), βE_0 (kJ mol^{-1}), and P_{0q} (atm), are 0.685,12.0, and 126 for **3** and 3.30, 8.13, and 129 for **5**, respectively. The βE_0 of **3** (12.0 kJ mol^{-1}) is larger than those (8−9 kJ $mmol^{-1}$) of molecular sieves,[67] activated carbon fibers,[66] and **5**. The highest adsorption energy of **3** in these porous materials is due to the small channel size of this network, which induces the enhancement in the intermolecular interaction between methane molecules and the channel network. These characters are also reflected to the rapid increase of the amount of adsorbed methane for **3** at lower pressure compared with that of **5**. Although **2** also has a methane adsorption activity, the isotherm is not the Langmuir-type but Henry-type. This could be associated with too small cross section of the channel for methane adsorption.

4·azpy adsorbs about 0.1 mmol of methane at a pressure of 36 atm,[68] while **1** adsorbs negligible amount of methane throughout the experiment, showing that these two compounds have no effective size of micropores for methane adsorption.

Thermal Stability of the Interpenetrated Network. The two-dimensional networks of azpy could form large voids due to the longer metal−metal distance than in the case of 4,4′-bpy, resulting in an interpenetration network. We found that the interpenetration networks still create microchannels, and adsorb methane gas molecules at room temperature. To elucidate the relationship between stability of porous structures and gas adsorption properties, thermal gravimetric (TG) analyses and measurements of the XRPD patterns were carried out. According to this analysis, the three types of networks are classified, which show the dependence of their robustness in the absence of included guest molecules: type I structure which retains no porosity with pore structure distortion, type II which retains porosity with pore structure distortion, and type III which retains porosity without structural distortion. For example **1** is classified type I, because the porous network of this compound deforms to lose the porous character upon removal of the guest ethanol molecules (see Experimental Section).

The TG curve of **3**·0.5EtOH illustrates release of the guest ethanol molecules up to 100 °C, followed by release of two azpy ligands from 150 to 200 °C and 280 to 320 °C. No chemical decomposition was observed between 100 °C and 150 °C. Similar TG pattern is observed for **2** and **5**.[69] Structures after removal of the guest water molecules in the channels were studied by the XRPD pattern under reduced pressure (<0.1 mmHg) at 100 °C; TG curves demonstrate that guest solvent molecules of these compounds are removed in this condition. Figure 7 shows the observed XRPD pattern of **3** under reduced pressure at 100 °C with the simulated powder pattern obtained upon removal of guest ethanol molecules from the single-crystal model. The good agreement of the both powder patterns reveals that the porous network is retained even in the absence of guest molecules. Therefore, this network is classified type III. Similar rigid porous structure has been obtained in the pillared-layer-type coordination polymer, $[Cu_2(pzdc)_2(L)]_n$ (pzdc = pyrazine-2,3-dicarboxylate, L = a pillar ligand),[12] whose network is three dimensionally linked by coordination bonds.

(64) Carlucci, L.; Ciani, G.; Proserpio, D. M. *New. J. Chem.* **1998**, 1319−1321.
(65) Kaneko, K.; Murata, K. *Adsorption* **1997**, *3*, 197−208.
(66) Kaneko, K.; Murata, K.; Shimizu, K.; Camara, S.; Suzuki, T. *Langmuir* **1993**, *9*, 1165−1167.
(67) Agaral, R. K.; Schwarz, J. A. *J. Colloid Interface Sci.* **1989**, *130*, 137.

(68) Under reduced pressure, a part of guest azpy of **4**·azpy sublimes to provide vacancies, in which a small amount of methane could be adsorbed.
(69) The TG curve of **2**·$2H_2O$ illustrates release of the guest water molecules up to 100 °C, followed by release of azpy molecules from 220 to 300 °C. The TG curve of **5**·$4H_2O$ illustrates release of the included water molecules up to 100 °C, followed by release of one azpy from 220 to 240 °C and two azpy ligands from 300 to 350 °C.

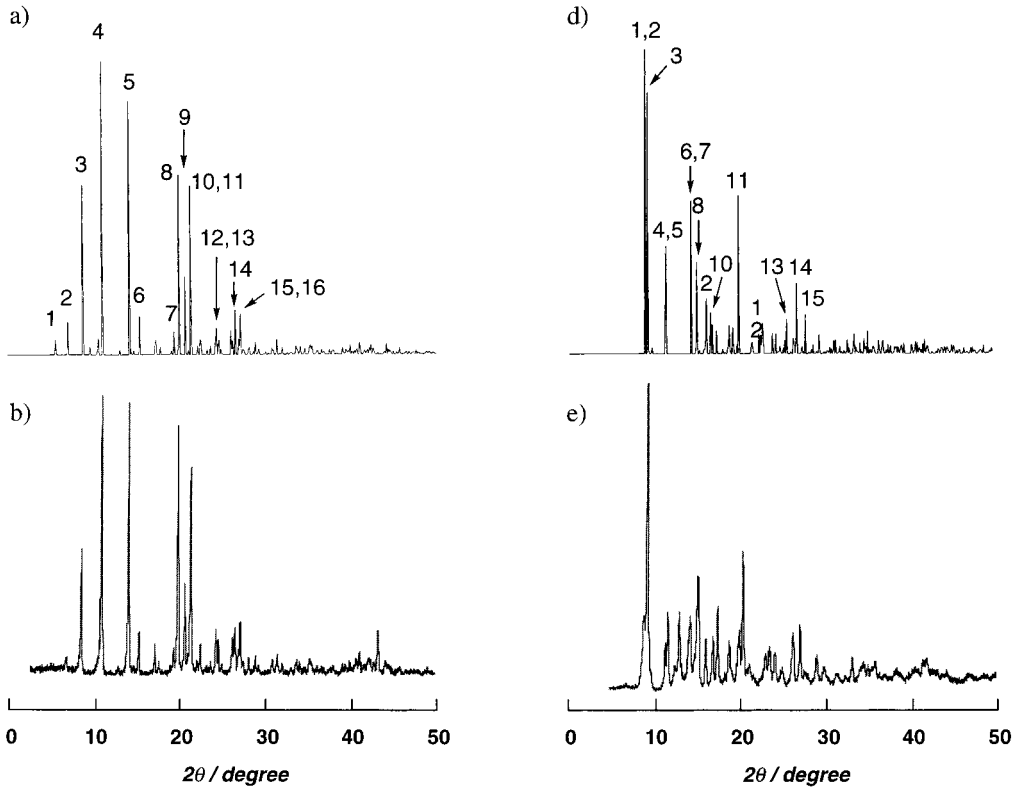

Figure 7. Simulated and observed XRPD pattern for **3** and **5** in the absence of guest molecules. (a) Simulated XRPD pattern upon removal of the ethanol from the single-crystal model of **3**·0.5EtOH. The main diffraction lines are indexed: 1 (020); 2 (111); 3 (002); 4 (220); 5 (042); 6 (241); 7 (260); 8 (243); 9 (421); 10 (402); 11 (262); 12 (173); 13 (064); 14 (264); 15 (354); and 16 (174). (b) The observed pattern of **3** under the reduced pressure at 100 °C. (c) Simulated XRPD pattern upon removal of the acetone from the single-crystal model of **5**·2Me_2CO. The main diffraction lines are indexed: 1 (11$\bar{1}$); 2 (110), 3 (20$\bar{2}$); 4 (11$\bar{2}$); 5 (111); 6 (31$\bar{2}$); 7 (31$\bar{2}$); 8 (112); 9 (021); 10 (20$\bar{4}$) 11 (22$\bar{3}$); 12 (51$\bar{1}$); 13 (402); 14 (42$\bar{5}$); and 15 (511). (d) The observed pattern of **5** under the reduced pressure at 100 °C.

Figure 7 also illustrates the observed XRPD pattern of **5** under reduced pressure at 100 °C and the simulated pattern based on the single-crystal model. Slight shifts of diffraction lines or the emergence of new diffraction lines are shown in the observed pattern of **5**. Similar shifts are already found when the sample was measured under reduced pressure at 27 °C. Although these results indicate the distortion of the network structure upon removal of guest molecules, the high activity of methane gas adsorption exhibits that the obtained network still retains a porous structure. Therefore, this network is classified type II.

The dried compound **2** has methane adsorption activity at room temperature. Although this dried compound was prepared under reduced pressure at 25 °C, the XRPD diffraction pattern of this compound under reduced pressure at 25 °C is not in agreement with the simulated pattern. This is due to the phase transition or deformation of the network structure upon loss of the guest solvent molecules. Moreover, most of diffraction lines are disappeared under reduced pressure at 100 °C, due to the formation of amorphous phase. This amorphous compound also shows Henry-type methane adsorption activity (0.33 mmol g^{-1} at 35 atm). The diffraction lines are not recovered under air for 1 h at room temperature. These results demonstrate that this compound classified type II. In conclusion, the interpenetrated networks of **2**, **3**, and **5** contribute to retaining the porous networks without guest molecules in the channels.

Concluding Remarks. Five new coordination networks, *logcabin* (**1**·2EtOH), *brick-wall* (**2**·Me_2CO·$3H_2O$), *rhombus-grid* (**3**·0.5EtOH), *square-grid* (**4**·azpy), and *herringbone* (**5**·2Me_2CO) types, have been constructed from a azpy ligand. Their solid-state structures were characterized by the single-crystal X-ray crystallography and XRPD measurements. In these compounds, the two-dimensional networks of **2**·Me_2CO·$3H_2O$, **3**·0.5EtOH, and **5**·2Me_2CO form the interpenetrated structures with microchannels, which are filled with guest solvent molecules. These porous structures are maintained after the removal of the guest molecules under reduced pressure. Their stable channels reversibly adsorb methane at ambient temperature. To the best of our knowledge, these are the first examples that the micropores, created by interpenetrated networks, adsorb small molecules such as methane at ambient temperature. This study demonstrates that the interpenetrated networks provide a good candidate for the construction of new functional microporous structures.

Acknowledgment. This work was supported by the Sumitomo Foundation and a Grant-in-Aid for Scientific Research from the Japanese Ministry of Education, Science, Sports, and Culture, Japan.

Supporting Information Available: Tables of crystallographic data, bond lengths and angles, and anisotropic parameters for the non-hydrogen atoms (PDF). This material is available free of charge via the Internet at http://pubs.acs.org.

CM990612M